Available online at www.sciencedirect.com
SCIENCE DIRECT®
Journal of Sound and Vibration 277 (2004) 223–238
JOURNAL OF SOUND AND VIBRATION
www.elsevier.com/locate/jsvi

Parametric stability of continuous shafts, connected to mechanisms with position-dependent inertia

O. Turhan*, K. Koser

Faculty of Mechanical Engineering, Istanbul Technical University, Gümüssuyu 80191, Istanbul, Turkey

Received 19 December 2002; accepted 28 August 2003

Abstract

Stability of the parametrically excited torsional vibrations of shafts connected to mechanisms with position-dependent inertia is studied via a version of Bolotin's method. The shafts are considered to be torsionally elastic, distributed parameter systems and discretized through a finite element scheme. The mechanisms are modelled by a linearized Eksergian equation of motion. A general method of analysis is described and applied to examples with slider–crank and Scotch-yoke mechanisms.

1. Introduction

The torsional vibrations of a shaft connected to a mechanism with position-dependent inertia, such as a linkage or cam mechanism, fall into the class of parametrically excited vibrations and, as such, have a multitude of otherwise unexpected resonance conditions. These are generally classified into two categories as parametric and combination resonances and the important problem of determining their occurrence conditions is referred to as dynamic stability analysis. More specifically, a stability analysis that deals only with parametric resonances is called parametric stability analysis in contrast to complete stability analysis where both parametric and combination resonances are considered.

Meyer zur Capellen [1] seems to be the first to give a comprehensive treatment of the problem. He considered a four bar mechanism with torsionally elastic input and output shafts, modelled the shafts as massless torsional springs carrying heavy flywheels, linearized the equation of motion of the mechanism and has shown that the motion of the system is governed by a system of Hill's equations. Along with other results, he presented those of a parametric stability analysis based on

*Corresponding author.
E-mail address: turhanoz@itu.edu.tr (O. Turhan).

0022-460X/$ - see front matter
doi:10.1016/j.jsv.2003.08.046

analog computer calculations. Later, Pasricha and Carnegie [2,3] considered the torsional vibrations of the crankshafts of reciprocating engines. They gave the linearized equations of motion of multi-cylinder engines [3] and presented a parametric stability analysis for the special case of a single-cylinder engine [2]. Zadoks and Midha [4,5] and Weyh and Kostyra [6,7] revisited the dynamic stability analysis problem of crank-shafts to provide (not only parametric, but) complete stability analyses via new and interesting methods. A single-cylinder engine was considered in Refs. [4,5] and up to six-cylinder engines were considered in Refs. [6,7]. The mathematical models used in Refs. [2–7] were similar to that described in Ref. [1]. Specifically, the crankshaft portions were always represented by massless torsional springs.

Unlike others, Koser and Pasin [8,9] considered the continuous model of a shaft driving a mechanism with position-dependent inertia and gave perturbation solutions for the forced torsional vibrations. A stability analysis could, however, not be performed due to the lack of a counterpart of Floquet theory in the area of partial differential equations.

The purpose of the present work is to introduce distributed parameter modelling of the shaft in the stability analysis of its torsional vibrations. To this end, a continuous shaft, carrying a heavy flywheel at one end, and connected to a mechanism with position dependent inertia at an arbitrary station is considered. A finite element discretization is then applied to the shaft, and the mechanism's non-linear Eksergian equation of motion is linearized about a non-oscillating nominal rotational motion. Application of a generalized Bolotin method given by Turhan [10] is described for complete stability analysis of the resulting multi-degrees-of-freedom discrete model. Numerical examples are given for shafts connected to slider–crank and Scotch-yoke mechanisms. But as the over-dimensionality of the problem prevented a complete stability analysis from being performed to an adequate degree of approximation, the numerical part of the study essentially remained in the framework of parametric stability analysis.

2. Formulation of the problem

Consider a torsionally elastic, circular cross-section shaft with mass density ρ, shear modulus G, polar area moment of inertia J_p and length ℓ, attached at one end to a flywheel with mass moment of inertia I_0 and connected, at a station k, to a mechanism whose generalized inertia can be expressed as

$$I(\varphi_k) = \bar{I} + \alpha\tilde{I}(\varphi_k), \tag{1}$$

where $\tilde{I}(\varphi_k)$ is a 2π periodic function of its argument (Fig. 1). Although it may also be interesting to study the effect of the flywheel inertia on the dynamics of the system, it will be assumed in this study that I_0 is large enough so that the left end of the shaft rotates at constant rate Ω_0. Whence $\varphi_0 = \bar{\varphi}_0 + \Omega_0 t$, where $\bar{\varphi}_0$ is an initial angular displacement.

Let a synthetical approach be adopted in the formulation of the equations of motion and, accordingly, consider first the mechanism and the shaft separately. Under the assumption that no force is acting on the mechanism, except the reaction torque—T of the shaft, the mechanism's equation of motion can be written as

$$I(\varphi_k)\cdot\ddot{\varphi}_k + \frac{1}{2}I'(\varphi_k)\cdot\dot{\varphi}_k^2 = -T, \tag{2}$$

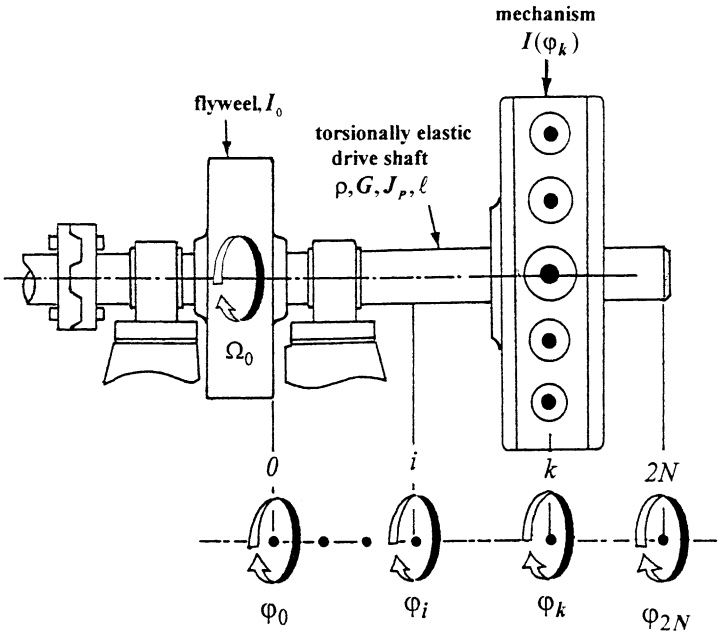

Fig. 1. System configuration.

where overdots denote differentiation with respect to time and primes denote differentiation with respect to φ_k. This equation, which is known in dynamics of machinery circles as the Eksergian equation of motion [11], is strongly non-linear. In order to linearize it, let one first introduce torsional co-ordinates θ to replace the rotational co-ordinates φ, so that for any ith station of the shaft

$$\varphi_i = \varphi_0 + \theta_i = \bar{\varphi}_0 + \Omega_0 t + \theta_i, \quad \dot{\varphi}_i = \Omega_0 + \dot{\theta}_i, \quad \ddot{\varphi}_i = \ddot{\theta}_i, \tag{3}$$

and assume that the time origin is so chosen that when $t = 0$ and $\theta_k = 0$ the mechanism is at its reference position $\varphi_k = 0$. Whence $\bar{\varphi}_0 = 0$. Then insert Eq. (3) into Eq. (2) whose left side thus becomes a function of the arguments $\theta_k, \dot{\theta}_k$ and $\ddot{\theta}_k$. Expand this function into a McLaurin series of its arguments and retain only linear terms (small torsional displacements assumption) to obtain

$$I(\Omega_0 t) \cdot \ddot{\theta}_k + I'(\Omega_0 t) \cdot \Omega_0 \cdot \dot{\theta}_k + \frac{1}{2} \cdot I''(\Omega_0 t) \cdot \Omega_0^2 \cdot \theta_k + \frac{1}{2} \cdot I'(\Omega_0 t) \cdot \Omega_0^2 = -T, \tag{4}$$

as the linearized equation of motion of the mechanism.

Next, consider the elastic shaft and let a discrete model of it be obtained via finite element method. Thus, divide the shaft into N elements with equal lengths, each possessing three nodes (one of which is an internal node placed at the middle), adopt a quadratic interpolation scheme, assume that the attachment point of the mechanism coincides with the kth node, introduce Rayleigh damping and obtain

$$\rho J_p \ell \cdot \mathbf{M} \cdot \ddot{\boldsymbol{\theta}} + (c_K \cdot \mathbf{K} + c_M \cdot \mathbf{M}) \cdot \dot{\boldsymbol{\theta}} + \frac{GJ_p}{\ell} \cdot \mathbf{K} \cdot \boldsymbol{\theta} = \mathbf{e}_k \cdot T, \tag{5}$$

as the equation of the torsional vibrations of the shaft. In Eq. (5), c_K and c_M are damping proportionality coefficients, $\boldsymbol{\theta} = \{\theta_1, \theta_2, \ldots, \theta_{2N}\}^{\mathrm{T}}$ is the $(2N \times 1)$ nodal co-ordinates matrix, $\mathbf{e}_k$ is the kth $2N$-dimensional unit vector such as $\mathbf{e}_3 = \{0, 0, 1, 0, 0, \ldots, 0\}^{\mathrm{T}}$ for example, and $\rho J_p \ell \cdot \mathbf{M}$ and $(GJ_p/\ell) \cdot \mathbf{K}$ are $(2N \times 2N)$ consistent, global mass and stiffness matrices obtained by taking into account the fact that $\theta_0 = 0$. The structures of the matrices $\mathbf{M}$ and $\mathbf{K}$ are given in Appendix A.

The equations of motion of the system can be obtained by substituting for T from Eq. (4) with $\theta_k = \mathbf{e}_k^{\mathrm{T}} \cdot \boldsymbol{\theta}$ into Eq. (5). Introducing the change of variable $\tau = \Omega_0 t$ $(= \varphi_0)$ and evoking Eq. (1) this yields, with $\Omega \neq 0$

$$[\mathbf{M} + [\beta + \lambda \tilde{I}(\tau)] \cdot \mathbf{e}_k \mathbf{e}_k^{\mathrm{T}}] \cdot \boldsymbol{\theta}'' + \left[\frac{2\zeta}{\Omega}(\mathbf{K} + \gamma \mathbf{M}) + \lambda \tilde{I}'(\tau) \cdot \mathbf{e}_k \mathbf{e}_k^{\mathrm{T}}\right] \cdot \boldsymbol{\theta}' + \left[\frac{1}{\Omega^2} \cdot \mathbf{K} + \frac{1}{2} \lambda \tilde{I}''(\tau) \cdot \mathbf{e}_k \mathbf{e}_k^{\mathrm{T}}\right] \cdot \boldsymbol{\theta} = -\frac{1}{2} \lambda \tilde{I}'(\tau) \cdot \mathbf{e}_k, \tag{6}$$

where primes denote differentiation with respect to τ, and the dimensionless parameters

$$\Omega = \frac{\Omega_0}{\sqrt{k^*/m^*}}, \quad \beta = \frac{\bar{I}}{m^*}, \quad \lambda = \frac{\alpha}{m^*}, \quad \zeta = \frac{c_K}{2\sqrt{k^* m^*}}, \quad \gamma = \frac{c_M}{c_K};$$
$$k^* = \frac{GJ_p}{\ell}, \quad m^* = \rho J_p \ell \tag{7}$$

are used.

3. Stability analysis

Eq. (6) constitutes a system of $2N$ Hill's equations with 2π periodic coefficients. A stability analysis can be carried out on its homogeneous part. To this end, let one first rearrange the equation by multiplying it from the left by the inverse of the coefficients' matrix of $\boldsymbol{\theta}''$, which according to Sherman–Morrison formula [12] can be written as

$$[\mathbf{M} + [\beta + \lambda \cdot \tilde{I}(\tau)] \cdot \mathbf{e}_k \mathbf{e}_k^{\mathrm{T}}]^{-1} = \left[\mathbf{M}^{-1} - \frac{\beta + \lambda \cdot \tilde{I}(\tau)}{1 + \mu_{kk} \cdot [\beta + \lambda \cdot \tilde{I}(\tau)]} \cdot \mathbf{M}^{-1} \cdot \mathbf{e}_k \mathbf{e}_k^{\mathrm{T}} \cdot \mathbf{M}^{-1}\right], \tag{8}$$

where $\mu_{kk} = \mathbf{M}^{-1}_{k,k}$, i.e. the kth row, kth column element of the inverse of $\mathbf{M}$. The result is

$$\boldsymbol{\theta}'' + \left[\mathbf{P}(\tau) + \frac{1}{\Omega} \cdot \mathbf{Q}(\tau)\right] \cdot \boldsymbol{\theta}' + \left[\mathbf{R}(\tau) + \frac{1}{\Omega^2} \cdot \mathbf{S}(\tau)\right] \cdot \boldsymbol{\theta} = \mathbf{0}, \tag{9}$$

where

$$\mathbf{P}(\tau) = \lambda \mathbf{A} \cdot [\mathbf{I} - \mathbf{A} \cdot f(\tau)] \cdot \tilde{I}'(\tau), \quad \mathbf{Q}(\tau) = 2\zeta[\mathbf{I} - \mathbf{A} \cdot f(\tau)] \cdot [\mathbf{B} + \gamma \mathbf{I}],$$
$$\mathbf{R}(\tau) = \frac{1}{2} \lambda \mathbf{A} \cdot [\mathbf{I} - \mathbf{A} \cdot f(\tau)] \cdot \tilde{I}''(\tau), \quad \mathbf{S}(\tau) = [\mathbf{I} - \mathbf{A} \cdot f(\tau)] \cdot \mathbf{B}, \tag{10}$$

with

$$\mathbf{A} = \mathbf{M}^{-1} \cdot \mathbf{e}_k \mathbf{e}_k^{\mathrm{T}}, \quad \mathbf{B} = \mathbf{M}^{-1} \mathbf{K}, \quad f(\tau) = \frac{\beta + \lambda \tilde{I}(\tau)}{1 + \mu_{kk}[\beta + \lambda \tilde{I}(\tau)]}. \tag{11}$$

Note that the use of Sherman–Morrison formula allowed the variable terms to be kept apart in the formulation. This feature is of great utility in numerical calculations.

The stability of the solutions of Eq. (9) will be studied via the Generalized Bolotin Method described in Ref. [10]. This method is based on the Floquet theory and gives the stability boundaries on a two-dimensional parameter space. Thus, evoke first the Floquet theory according to which a solution of Eq. (9) can be written as a product of an exponential part and a 2π periodic part. Representing the periodic part by its complex Fourier series expansion, this solution can be written as

$$\boldsymbol{\theta}(\tau) = \mathbf{e}^{\rho\tau} \sum_{r=-\infty}^{\infty} \mathbf{D}_r \mathbf{e}^{\mathrm{i}r\tau}, \tag{12}$$

where ρ represents the Floquet (or characteristic) exponent and $\mathbf{D}_r$'*s* are unknown $2N \times 1$ complex Fourier coefficients' matrices. Inserting solution (12) into Eq. (9), representing the 2π periodic matrices $\mathbf{P}(\tau)$, $\mathbf{Q}(\tau)$, $\mathbf{R}(\tau)$ and $\mathbf{S}(\tau)$ by their complex Fourier series expansions up to the *m*th harmonic, and collecting equal powers of $\mathbf{e}^{\mathrm{i}\tau}$, Eq. (9) gives

$$(\rho + \mathrm{i}r)^2 \mathbf{D}_r + \sum_{p=-m}^{m} \left[(\rho + \mathrm{i}q)(\mathbf{P}_p + \frac{1}{\Omega}\mathbf{Q}_p) + (\mathbf{R}_p + \frac{1}{\Omega^2}\mathbf{S}_p) \right] \mathbf{D}_q = \mathbf{0},$$
$$r = \ldots, -2, -1, 0, 1, 2, \ldots, \quad q = r - p, \tag{13}$$

where $\mathbf{P}_p$, $\mathbf{Q}_p$, $\mathbf{R}_p$ and $\mathbf{S}_p$ are the *p*th complex Fourier coefficients' matrices of the related matrices. Eq. (13) constitutes an infinite system of homogeneous algebraic equations for the unknown vectors $\mathbf{D}_r$. This system may conveniently be written in a hyper-matrix/vector form as

$$\left[\rho^2 \mathbf{I} + \rho \left[\mathbf{E}_0 + \frac{1}{\Omega}\mathbf{E}_1 \right] + \left[\mathbf{F}_0 + \frac{1}{\Omega}\mathbf{F}_1 + \frac{1}{\Omega^2}\mathbf{F}_2 \right] \right] \mathbf{D} = \mathbf{0}, \tag{14}$$

where $\mathbf{D}$ is an infinite hyper-vector defined as $\mathbf{D} = \{\ldots, \mathbf{D}_{-2}^{\mathrm{T}}, \mathbf{D}_{-1}^{\mathrm{T}}, \mathbf{D}_0^{\mathrm{T}}, \mathrm{D}_1^{\mathrm{T}}, \mathbf{D}_2^{\mathrm{T}}, \ldots\}^{\mathrm{T}}$, $\mathbf{I}$ is the infinite-dimensional unit matrix and $\mathbf{E}_i$, $\mathbf{F}_i$'s are infinite-dimensional hyper-matrices made up of $2N \times 2N$ sub-matrices given by

$$\mathbf{E}_0^{r,q} = \mathbf{P}_p + 2\mathrm{i}r\mathbf{I}\delta_{rq}, \quad \mathbf{E}_1^{r,q} = \mathbf{Q}_p,$$
$$\mathbf{F}_0^{r,q} = \mathbf{R}_p + \mathrm{i}q\mathbf{P}_p - r^2\mathbf{I}\delta_{rq}, \quad \mathbf{F}_1^{r,q} = \mathrm{i}q\mathbf{Q}_p, \quad \mathbf{F}_2^{r,q} = \mathbf{S}_p, \tag{15}$$

where δ_{rq} is the Kronecker delta and the superscripts r and q refer to the hyper-row and column indices. In order for Eq. (9) to admit a non-trivial solution of form (12), the determinant of the coefficients' matrix of Eq. (14) must vanish:

$$\det \left[\rho^2 \mathbf{I} + \rho \left[\mathbf{E}_0 + \frac{1}{\Omega}\mathbf{E}_1 \right] + \left[\mathbf{F}_0 + \frac{1}{\Omega}\mathbf{F}_1 + \frac{1}{\Omega^2}\mathbf{F}_2 \right] \right] = 0. \tag{16}$$

This equation can be used to calculate the Ω values corresponding to stability boundaries on a parameter space, which has Ω as one of its components, provided that the value of the Floquet exponent ρ on those boundaries is known. In fact, it is known that on harmonic and sub-harmonic parametric resonance boundaries a certain *s*th exponent takes, respectively, the values

$$\rho_s = 0, \tag{17}$$

and

$$\rho_s = \frac{i}{2}. \tag{18}$$

Furthermore, it can be shown [10] that for a non-canonical system such as the one considered here, on a combination resonance boundary a certain pair (ρ_s, ρ_t); $s \neq t$ of Floquet exponents take values so that

$$\rho_s + \rho_t = 0. \tag{19}$$

Whence, putting $\rho = 0$ from Eq. (17) into Eq. (16), one has for harmonic parametric resonance boundaries

$$\det\left[\mathbf{F}_0 + \frac{1}{\Omega}\mathbf{F}_1 + \frac{1}{\Omega^2}\mathbf{F}_2\right] = 0, \tag{20}$$

and putting $\rho = i/2$ from Eq. (18) into Eq. (16) one has for sub-harmonic parametric resonance boundaries

$$\det\left[\left[\mathbf{F}_0 + \frac{i}{2}\mathbf{E}_0 - \frac{1}{4}\mathbf{I}\right] + \frac{1}{\Omega}\left[\mathbf{F}_1 + \frac{i}{2}\mathbf{E}_1\right] + \frac{1}{\Omega^2}\mathbf{F}_2\right] = 0, \tag{21}$$

while for combination resonance boundaries, first linearize the matrix polynomial of Eq. (16), which is a monic matrix polynomial of second degree in ρ, to obtain the Hill's determinant of the problem

$$\det\left[\left[\mathbf{U}_0 + \frac{1}{\Omega}\mathbf{U}_1 + \frac{1}{\Omega^2}\mathbf{U}_2\right] - \rho\mathbf{I}\right] = 0, \tag{22}$$

where

$$\mathbf{U}_0 = \begin{bmatrix} -\mathbf{E}_0 & -\mathbf{F}_0 \\ \mathbf{I} & \mathbf{0} \end{bmatrix}, \quad \mathbf{U}_1 = \begin{bmatrix} -\mathbf{E}_1 & -\mathbf{F}_1 \\ \mathbf{0} & \mathbf{0} \end{bmatrix}, \quad \mathbf{U}_2 = \begin{bmatrix} \mathbf{0} & -\mathbf{F}_2 \\ \mathbf{0} & \mathbf{0} \end{bmatrix}. \tag{23}$$

Then introduce the bi-alternate sum matrices $\mathbf{B}(\mathbf{U}_i)$ of the matrices $\mathbf{U}_i$, which have the property of having as eigenvalues, the sums of the eigenvalues of the argument matrix taken in pairs [13] (see Refs. [10] or [13] for the construction of these matrices) and write in view of Eqs. (19) and (22)

$$\det\left[\mathbf{B}(\mathbf{U}_0) + \frac{1}{\Omega}\mathbf{B}(\mathbf{U}_1) + \frac{1}{\Omega^2}\mathbf{B}(\mathbf{U}_2)\right] = 0, \tag{24}$$

for combination resonance boundaries. Ω values corresponding to stability boundaries can be calculated from Eqs. (20), (21) and (24) by solving an eigenvalue analysis problem. To this end, note that all the three equations are of the form

$$\det\left[\mathbf{M}_0 + \frac{1}{\Omega}\mathbf{M}_1 + \frac{1}{\Omega^2}\mathbf{M}_2\right] = 0, \tag{25}$$

thus, involving matrix polynomials of second degree in $1/\Omega$. Multiplying by Ω^2 and linearizing, one may write

$$\det\left[\begin{bmatrix} -\mathbf{M}_0^{-1}\mathbf{M}_1 & -\mathbf{M}_0^{-1}\mathbf{M}_2 \\ \mathbf{I} & \mathbf{0} \end{bmatrix} - \Omega\mathbf{I}\right] = 0, \tag{26}$$

whenever $\mathbf{M}_0$ is invertible. When this is not the case, first put $1/\Omega = 1/\bar{\Omega} + 1/\delta$ (where $1/\delta$ is a scalar not equalling a proper value of the matrix polynomial in question) into Eq. (25) and solve Eq. (26) with

$$\bar{\mathbf{M}}_0 = \mathbf{M}_0 + \frac{1}{\delta}\mathbf{M}_1 + \frac{1}{\delta^2}\mathbf{M}_2, \quad \bar{\mathbf{M}}_1 = \mathbf{M}_1 + \frac{1}{2\delta}\mathbf{M}_2, \quad \bar{\mathbf{M}}_2 = \mathbf{M}_2, \tag{27}$$

for $\bar{\Omega}$, and then calculate Ω as $\Omega = \delta\bar{\Omega}/(\delta + \bar{\Omega})$.

Now, a few words on the implementation of the above-described method are in order. First, let one note that, if the Fourier series of the solution given in equation (12) is truncated at the Rth harmonic (meaning that approximations for up to the Rth order instability regions will be obtained, the last ones being the least reliable), the order of the eigenvalue analysis problem of Eqs. (20) and (21) is $\eta_1 = 4N(2R + 1)$ and that of the Eq. (24) is $\eta_2 = \eta_1(\eta_1 - 1)$, where N is the finite element number used in modelling the shaft. Notice that these dimensions may grow prohibitive for large values of N and R. Second, one should realize that all the Ω values calculated through Eqs. (20), (21) and (24) are not admissible. One has to eliminate (a) those Ω values that are not real numbers, and (b) those corresponding to unconverged (ρ_s, ρ_t) pairs or to pairs whose imaginary parts violate the inequality $-\frac{1}{2} < \mathrm{Im}(\rho_{s,t}) < \frac{1}{2}$. Condition (a) that follows from obvious physical considerations applies to any of problems (20), (21) and (26), and its implementation does require no additional effort. Condition (b) is ultimately related to the redundant and periodic (i periodic in ρ) nature of the Hill's determinant of Eq. (22). As a result of this, an η_1th order segment of it, gives Rth order approximations to the $4N$ Floquet exponents ρ; $-\frac{1}{2} \leqslant \mathrm{Im}(\rho) \leqslant \frac{1}{2}$ of the problem, and diminishing order approximations to their congruents $\rho \pm ri$; $r = 1, 2, \ldots, R$. A calculated Floquet exponent can be qualified as converged if it satisfies the above-mentioned inequality and its first congruent also appear to within a prescribed tolerance. Thus, condition (b) applies only to problem (26) and its implementation requires the corresponding ρ values be calculated through Eq. (22).

4. Applications

The above-described method has been applied to two different examples, in the first of which the shaft is connected to a slider–crank mechanism and in the second to a Scotch-yoke mechanism. The calculations are performed by means of a special FORTRAN code developed for implementing the proposed method.

4.1. Shaft connected to a slider–crank mechanism

Let the shaft be connected to a centric slider–crank mechanism attached to its right end so that the attachment station number is $k = 2N$. Although an exact analysis is also possible, let the generalized inertia $I(\tau)$ of the mechanism be determined in an approximate sense. To this end, consider the slider–crank mechanism depicted in Fig. 2 and introduce the following assumptions: (i) assume that the connecting rod is designed so that $\ell_A(\ell - \ell_A) = i_{S_3}^2$ where i_{S_3} is the centroidal radius of gyration. Under this assumption, which is at least approximately true for most high-speed slider–crank mechanisms, the slider-connecting rod sub-system is dynamically equivalent to

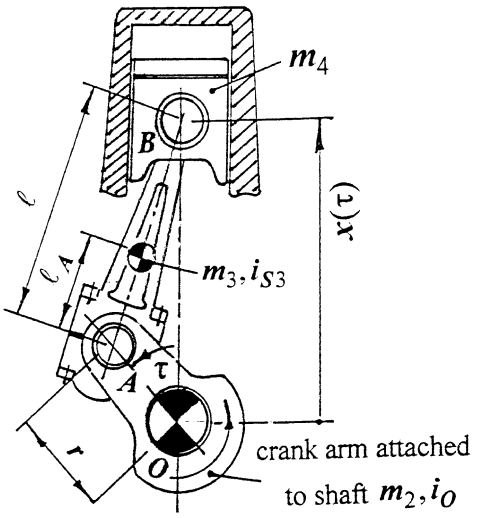

Fig. 2. Slider–crank mechanism.

the point masses

$$m_A = \left(1 - \frac{\ell_A}{\ell}\right) \cdot m_3, \quad m_B = \frac{\ell_A}{\ell} \cdot m_3 + m_4, \tag{28}$$

placed at the joints A and B, respectively. (ii) Assume that the ratio $\mu = r/\ell$ is small enough (It is at the order of $\frac{1}{4}\frac{1}{5}$ in most practical slider–crank mechanisms.), so that the slider position whose exact expression is $x(\tau) = r\cos\tau + \ell\sqrt{1 - \mu^2 \sin^2\tau}$ can be approximated by

$$x(\tau) = r\cos\tau + \ell\left(1 - \frac{1}{2}\mu^2 \sin^2\tau\right), \tag{29}$$

obtained by expanding the exact expression into a binomial series and neglecting higher than the second order terms in μ. Under these assumptions, one obtains, after necessary calculations

$$\bar{I} = m_2 i_0^2 + \left[m_A + \frac{m_B}{2}\left(1 + \frac{\mu^2}{4}\right)\right] \cdot r^2, \quad \alpha = \frac{1}{2} m_B r^2,$$

$$\tilde{I}(\tau) = \mu\cos\tau - \cos 2\tau - \mu\cos 3\tau - \frac{\mu^2}{4}\cos 4\tau, \tag{30}$$

where i_0 is the crank arm's radius of gyration with respect to the fixed pivot O.

Prior to the stability analysis, the dimensionless natural frequencies $\bar{\omega}_i = \sqrt{\rho\ell^2/G} \cdot \omega_i$, $i = 1, 2, \ldots$ of a shaft fixed at one end and carrying a disk of constant moment of inertia $\bar{I}$ at the other are calculated through FEM for different values of element number N and of moment of inertia ratio β. These results are compared on Table 1 to those obtained by solving the exact frequency equation

$$\cos\bar{\omega} - \beta\,\bar{\omega}\sin\bar{\omega} = 0. \tag{31}$$

Table 1
Comparison of FEM and exact natural frequency calculations

	ϖ_1	ϖ_2	ϖ_3	ϖ_4	ϖ_6	ϖ_8	ϖ_{10}
$\beta = 0$							
$N = 2$	1.571199	4.790216	8.778561	14.096046	—	—	—
$N = 5$	1.570807	4.714858	7.883466	11.138199	18.717519	28.364020	38.107046
$N = 10$	1.570797	4.712549	7.855993	11.006081	17.371554	23.951078	30.702345
$N = 20$	1.570796	4.712399	7.854110	10.996261	17.285195	23.591362	29.937389
Exact	1.570796	4.712389	7.853982	10.995574	17.278760	23.561945	29.845130
$\beta = 1$							
$N = 2$	0.860354	3.444298	6.487839	11.436766	—	—	—
$N = 5$	0.860334	3.426133	6.448698	9.603700	15.878412	25.697553	36.405206
$N = 10$	0.860334	3.425651	6.438051	9.534555	15.831526	22.325413	29.128519
$N = 20$	0.860334	3.425621	6.437346	9.529672	15.775389	22.057731	28.381250
Exact	0.860334	3.425618	6.437298	9.529334	15.771285	22.036497	28.309643
$\beta = 5$							
$N = 2$	0.432841	3.217025	6.357470	11.364069	—	—	—
$N = 5$	0.432841	3.204303	6.325174	9.516738	15.824612	25.664293	36.396098
$N = 10$	0.432841	3.203958	6.315530	9.450941	15.779908	22.286220	29.090290
$N = 20$	0.432841	3.203936	6.314889	9.446271	15.724723	22.021296	28.352641
Exact	0.432841	3.203935	6.314846	9.445948	15.720685	22.000239	28.281406

Inspection of this table shows that even $N = 2$ may be enough for accurate prediction of the fundamental frequency but in order to have a first few natural frequencies accurately predicted one has to use at least $N = 5$ elements. This implies that no less than 5 elements should be used in a stability analysis where the effects of higher modes are to be considered.

Stability analysis results will be presented in the form of stability charts constructed on a Ω–λ parameter plane. The frequencies given in Table 1 will also be useful in predicting the locations of the resonance regions on these charts. To this end it suffices to recall that, in the absence of damping, the kth order harmonic and sub-harmonic parametric resonance regions of the ith mode will emanate, respectively, from the points

$$\Omega_{ik}^{\mathrm{H}} = \frac{\bar{\omega}_i}{k}, \quad \Omega_{ik}^{\mathrm{S}} = \frac{2\bar{\omega}_i}{(2k-1)}; \quad k = 1, 2, \ldots, R, \tag{32}$$

of the Ω axis, while the kth order sum and difference type combination resonance regions of the i and jth modes will emanate from

$$\Omega_{ijk}^{C\pm} = \frac{\bar{\omega}_j \pm \bar{\omega}_i}{k}; \quad j > i. \tag{33}$$

For stability analysis, a numerical example with $\mu = 0.25$, $\beta = 1$, $\zeta = 0.0001$, $\gamma = 1$ is considered. $m = 4$ is set in Eq. (13) in consistency with Eq. (30) where a four harmonics approximation is adopted for $\tilde{I}(\tau)$. The elements of the complex Fourier coefficients' matrices $\mathbf{P}_p$,

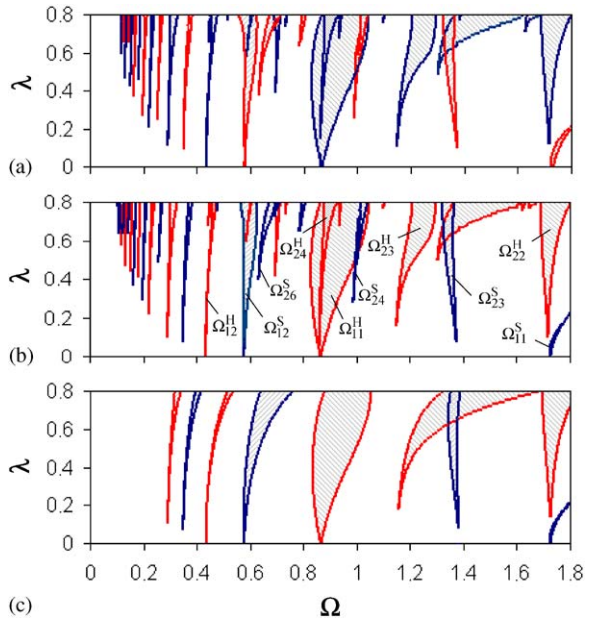

Fig. 3. Parametric stability charts with different N and R values. (a) $N = 20, R = 10$, (b) $N = 5, R = 10$, (c) $N = 2, R = 3$ (Slider–crank; $\mu = 0.25$, $\beta = 1$, $\zeta = 0.0001$, $\gamma = 1$) (\\\: harmonic, ///: sub-harmonic resonance zones).

$\mathbf{Q}_p$, $\mathbf{R}_p$ and $\mathbf{S}_p$, $p = -4, -3, \ldots, 0, \ldots, 3, 4$ are calculated through numerical integration by using Simpson's rule.

First, Ω values corresponding to parametric resonance boundaries are calculated from Eqs. (20) and (21) for given λ values and with different values of element number N and truncation number R of the Fourier series of Eq. (12). After a number of trials it has been seen that parametric stability analysis results converge, in a broad range of the parameters Ω and λ, when these values are set to $N = 20$ and $R = 10$. Figs. 3(a)–(c) depict stability charts obtained with three different combinations of N and R. The charts contain velocity ranges at the order of the fundamental resonance frequency $\varpi_1 = 0.860334$ (see Table 1, $\beta = 1$). An inspection of these figures shows that the combination $N = 5$, $R = 10$ (Fig. 3(b)) is adequate in the considered parameter range, in the sense that in that range its results closely simulate those obtained with $N = 20$, $R = 10$ (Fig. 3(a)). It may also be seen that the combination $N = 2$, $R = 3$ (Fig. 3(c)) is satisfactory in predicting the fundamental harmonic resonance region but not elsewhere. These results are in accordance with those obtained by inspecting Table 1 and imply that at least $N = 5$, $R = 10$ should be used in the analysis. But, matrix dimensions are then $\eta_1 = 420$ in parametric stability analysis (Eqs. (20) and (21)) and $\eta_2 = 175980$ in the determination of the boundaries of combination resonance regions (Eq. (24)). As the value of η_2 is beyond acceptable limits, the determination problem of the combination resonance regions could, unfortunately, not be solved at that level of approximation. It has been decided, therefore, to give for each problem, a relatively accurate parametric stability chart obtained with $N = 5$, $R = 10$ accompanied with a coarse approximation complete stability chart obtained with $N = 2$, $R = 3$ ($\eta_1 = 56, \eta_2 = 3080$). Though not of desired accuracy, this latter will give an idea on the combination resonances, which will prove to be effective in the considered problem class.

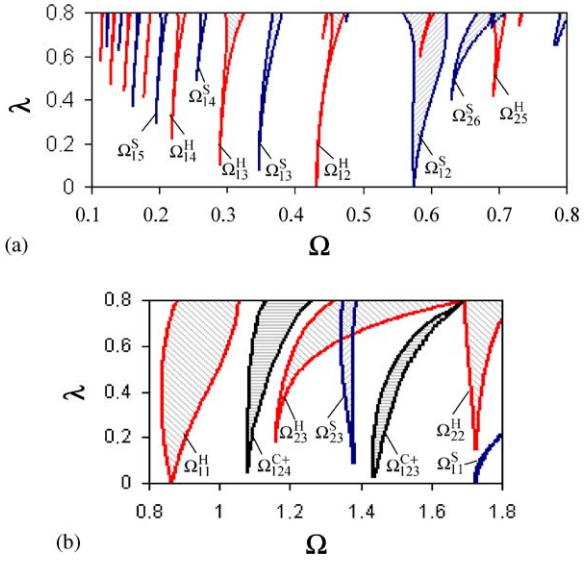

Fig. 4. Stability charts for slider–crank ($\mu = 0.25, \beta = 1, \zeta = 0.0001, \gamma = 1$). (a) Detail from Fig. 3(b), (b) complete analysis (coarse approximation) (\\\: harmonic, ///: sub-harmonic, ≡: combination resonance zones).

Fig. 4(a) is a zoom to the lower velocity ranges of the parametric stability chart of Fig. 3(b), and Fig. 4(b) is the coarse approximation complete stability chart, in the sense described above. To facilitate interpretation of these charts, some of the unstable zones (cross-hatched regions) are labelled according to their emanation points as described in Eqs. (32) and (33).

An inspection of Figs. 3 and 4 shows that spread out among the instability zones of the first torsional mode, are numerous parametric resonance zones related to higher modes and considerable combination resonance zones. Moreover, some of these zones, such as Ω^{H}_{25} and Ω^{S}_{26} for example (see Fig. 4(a)), range below the fundamental resonance frequency. Noting that these resonances could not be predicted through a massless shaft model, one concludes that continuous modelling of the shaft is indispensable for a thorough stability analysis of the considered system.

On the other hand, one notes from Fig. 4(a) that up to the sixth order instability regions of the first mode attain an observable width in the considered range of λ. This implies that rotation rates as low as one-sixth of the fundamental torsional natural frequency of the shaft may be unsafe for the considered example, which is very slightly damped ($\zeta = 0.0001$).

Fig. 5 corresponds to a damping factor value of $\zeta = 0.01$ and shows the effect of damping on the stability of the above considered shaft. Comparing Figs. 3–5 one concludes that the most obvious effects of damping are to eliminate the higher order instability regions with small width and to push all the instability regions towards larger λ values by rounding the points of the instability horns. Thus, damping has a stabilizing effect on the torsional vibrations of the shaft. It should, however, be noted that the Rayleigh damping model adopted in this study is rather of a formal nature and that, as compared to the actual material damping, it has the tendency of exaggerating the effect of damping with increasing Ω.

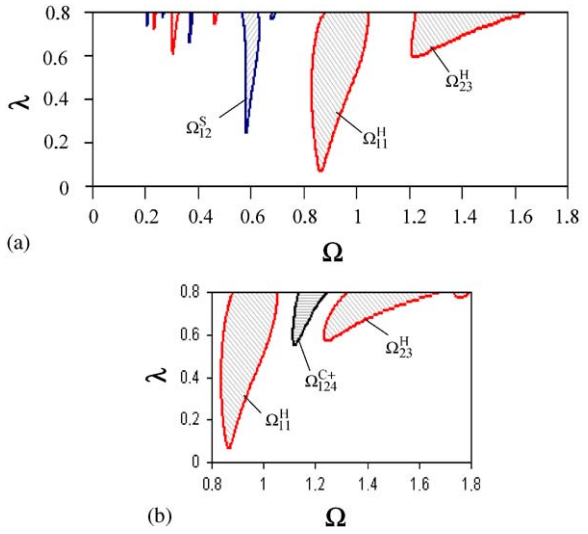

Fig. 5. Stability charts for slider–crank ($\mu = 0.25, \beta = 1, \zeta = 0.01, \gamma = 1$). (a) Parametric, (b) complete (coarse approximation) (\\\: harmonic, ///: sub-harmonic, ≡: combination resonance zones).

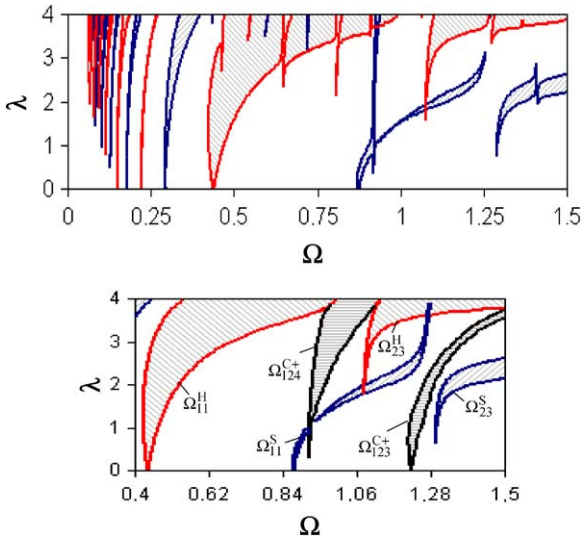

Fig. 6. Stability charts for slider–crank ($\mu = 0.25, \beta = 5, \zeta = 0.0001, \gamma = 1$). (a) Parametric, (b) complete (coarse approximation) (\\\: harmonic, ///: sub-harmonic, ≡: combination resonance zones).

Finally, Fig. 6 shows stability charts of the above example with $\zeta = 0.0001$ and $\beta = 5$. Comparing to Figs. 3 and 4 one notes that the instability regions are now shifted towards smaller Ω values, this effect being especially pronounced for the instability regions related to the first torsional mode. This is due to the fact that the fundamental frequency is now reduced to $\varpi_1 = 0.432841$ (see Table 1, $\beta = 5$). Also, as the first two natural frequencies of the shaft are now better

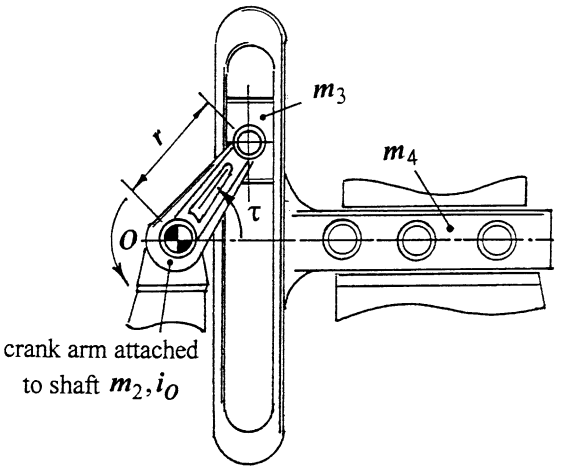

Fig. 7. Scotch-yoke mechanism.

separated, the parameter ranges dominated by the instability zones of the fundamental mode are now less subjected to the intervention of those of the second mode.

4.2. *Shaft connected to a Scotch-yoke mechanism*

Let the shaft be connected to a Scotch-yoke mechanism (Fig. 7) attached again at its right end ($k = 2N$). For this simple mechanism one has

$$\bar{I} = m_2 i_0^2 + \left(m_3 + \frac{m_4}{2}\right) r^2, \quad \alpha = \frac{1}{2} m_4 r^2, \quad \tilde{I}(\tau) = -\cos 2\tau, \tag{34}$$

where i_0 is the second link's radius of gyration with respect to the fixed pivot O.

Two numerical examples are considered where $\zeta = 0.0001$ and $\gamma = 1$. $m = 8$ is set in Eq. (13) and again $N = 5$, $R = 10$ are taken in parametric stability analysis while taking $N = 2$, $R = 3$ in complete stability analysis. The first example corresponds to $\beta = 1$ and the resulting stability charts are given in Figs. 8(a) and (b). A portion $\Omega < 0.4$ of the stability chart is not shown on Fig. 8(a) because no instability region of observable width has been obtained in that region. Also, no sub-harmonic parametric resonance region of finite width has been obtained for this example. Comparing Figs. 8(a) and (b) to their counterparts with slider–crank mechanism (Figs. 3(b) and 4(b)) one observes that there is a certain resemblance with respect to harmonic resonances but that, in general, the shaft with Scotch-yoke mechanism is less prone to go unstable. The second example corresponds to $\beta = 5$ and the resulting stability charts are given in Figs. 9(a) and (b). It can be seen that sub-harmonic resonance regions are now present, most of them being in the curious form of "S"-shaped narrow bands (Fig. 9(a)).

Before closing this section, let one redraw attention to the existence of well-pronounced combination resonance regions in all of the considered cases (Figs. 4(b), 5(b), 6(b),8(b), 9(b)) and note that this feature is not shared by any practical dynamic stability analysis problem.

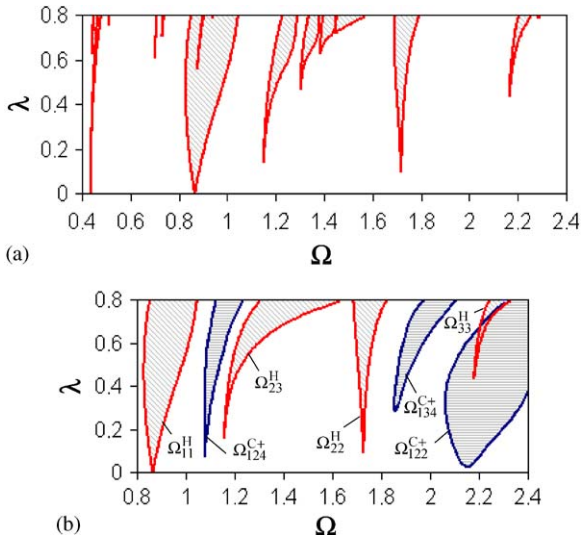

Fig. 8. Stability charts for scotch–yoke ($\beta = 1, \zeta = 0.0001, \gamma = 1$). (a) Parametric, (b) complete (coarse approximation) (\\\: harmonic, ≡: combination resonance zones).

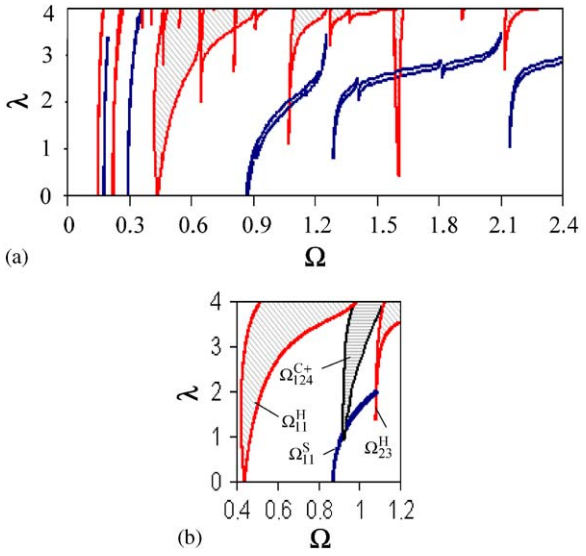

Fig. 9. Stability charts for scotch–yoke ($\beta = 5, \zeta = 0.0001, \gamma = 1$). (a) Parametric, (b) complete (coarse approximation) (\\\: harmonic, ///: sub-harmonic, ≡: combination resonance zones).

5. Conclusions

A general method of dynamic stability analysis is described for FEM-modelled continuous shafts connected to mechanisms with position dependent inertia. Numerical examples are given for shafts connected to slider–crank and Scotch-yoke mechanisms. In the numerical examples, the

determination problem of the combination resonances could, however, not be considered to a desired degree of accuracy, due to its over-dimensionality.

The considered examples have shown that both parametric and combination resonances related to higher torsional modes of the shaft have considerable effects on its stability performance. Moreover, when the system is slightly damped and the constant part of the generalized inertia of the attached mechanism is relatively small (so that the first two natural frequencies of the shaft are not well separated) these effects can be observed at velocity ranges where the resonance zones of the first mode are expected to dominate. It is, therefore, concluded that continuous modelling of the shaft is indispensable for a thorough stability analysis of its torsional vibrations.

Among the two considered mechanisms, the slider–crank is determined to be the worst in the sense that it has a stronger destabilizing effect on its shaft. It is shown that for a shaft connected at one end to that kind of mechanism, rotation rates as low as one-sixth of the fundamental torsional frequency may be unsafe if no sufficient damping is present.

Appendix A

Details of construction of global mass and stiffness matrices in the analysis of torsional (or longitudinal) vibrations of prismatic bars can be found in many textbooks (see for example, Ref. [14]). The non-dimensional parts of these matrices, corresponding to quadratic interpolation function, internal node placed at the middle of each element, consistent mass matrix, bar with left end fixed and element number N (matrix dimensions: $2N \times 2N$), are reproduced here for completeness.

$$\mathbf{K} = \frac{N}{3} \cdot \begin{bmatrix} 16 & -8 & & & & & & \\ -8 & 14 & -8 & 1 & & & \mathbf{0} & \\ & -8 & 16 & -8 & & & & \\ & 1 & -8 & 14 & -8 & 1 & & \\ & & & & \ddots & & & \\ & & & 1 & -8 & 14 & -8 & 1 \\ & \mathbf{0} & & & & -8 & 16 & -8 \\ & & & & & 1 & -8 & 7 \end{bmatrix}, \tag{A.1}$$

$$\mathbf{M} = \frac{1}{30N} \cdot \begin{bmatrix} 16 & 2 & & & & & & \\ 2 & 8 & 2 & -1 & & & \mathbf{0} & \\ & 2 & 16 & 2 & & & & \\ & -1 & 2 & 8 & 2 & -1 & & \\ & & & & \ddots & & & \\ & & & -1 & 2 & 8 & 2 & -1 \\ & \mathbf{0} & & & & 2 & 16 & 2 \\ & & & & & -1 & 2 & 4 \end{bmatrix}. \tag{A.2}$$

References

[1] W. Meyer zur Capellen, Torsional vibrations in the shafts of linkage mechanisms, *Journal of Engineering for Industry* 89 (1) (1967) 126–136.
[2] M.S. Pasricha, W.D. Carnegie, Effects of variable inertia on the damped torsional vibrations of Diesel engine systems, *Journal of Sound and Vibration* 46 (3) (1976) 339–345.
[3] M.S. Pasricha, W.D. Carnegie, Formulation of the equations of dynamic motion including the effects of variable inertia on the torsional vibrations in reciprocating engines, Part 1, *Journal of Sound and Vibration* 66 (2) (1979) 181–186.
[4] R.I. Zadoks, A. Midha, Parametric stability of a two-degree-of-freedom machine system: part I—equations of motion and stability, *Journal of Mechanisms, Transmissions, and Automation in Design* 109 (1987) 210–215.
[5] R.I. Zadoks, A. Midha, Parametric stability of a two-degree-of-freedom machine system: part II—stability analysis, *Journal of Mechanisms, Transmissions, and Automation in Design* 109 (1987) 216–223.
[6] B. Weyh, H. Kostyra, Direct Floquet method for stability limits determination—I: theory, *Mechanism and Machine Theory* 26 (1991) 123–131.
[7] H. Kostyra, B. Weyh, Direct Floquet method for stability limits determination—II: application and phenomena, *Mechanism and Machine Theory* 26 (1991) 123–131.
[8] K. Koser, F. Pasin, Continuous modelling of the torsional vibrations of the drive shaft of mechanisms, *Journal of Sound and Vibration* 188 (1) (1995) 17–24.
[9] K. Koser, F. Pasin, Torsional vibrations of the drive shafts of mechanisms, *Journal of Sound and Vibration* 199 (4) (1997) 559–565.
[10] Ö. Turhan, A generalized Bolotin's method for stability limit determination of parametrically excited systems, *Journal of Sound and Vibration* 216 (5) (1998) 851–863.
[11] B. Paul, *Kinematics and Dynamics of Planar Machinery*, Prentice-Hall, Englewood Cliffs, NJ, 1979.
[12] J. Sherman, W.J. Morrison, Adjustment of an inverse matrix corresponding to a change in one element of a given matrix, *Annals of Mathematical Statistics* 21 (1) (1950) 124–127.
[13] A.T. Fuller, Conditions for a matrix to have only characteristic roots with negative real parts, *Journal of Mathematical Analysis and Applications* 23 (1968) 71–98.
[14] L. Meirovitch, *Elements of Vibration Analysis*, Second Edition, McGraw-Hill, New York, 1986.